VARIANCE REDUCTION STRATEGIES FOR IMPLICIT MONTE CARLO SIMULATIONS

A Thesis

by

JACOB TAYLOR LANDMAN

Submitted to the Office of Graduate and Professional Studies of
Texas A&M University
in partial fulfillment of the requirements for the degree of

MASTER OF SCIENCE

Chair of Committee,	Ryan G. McClarren
Committee Members,	Jim E. Morel
	Prabir Daripa
Head of Department,	Yassin A. Hassan

December 2016

Major Subject: Nuclear Engineering

ABSTRACT

The thermal radiative transfer equations are extremely complex to solve; however, accurate solutions are necessary for problems concerning inertial confinement fusion and radiation hydrodynamics (e.g. supernova explosions). A method known as Implicit Monte Carlo (IMC) is widely used among the scientific community to solve such problems; however, the slow convergence of Monte Carlo methods can result in exhaustion of computational resources and statistically inaccurate solutions for very complex simulations. Thus, methods must be developed to decrease the uncertainty in our results without exhausting our resources.

In this work, we developed, tested, and analyzed two methods that aim to reduce uncertainty and increase the efficiency of the IMC method. The first method intends to remove an anomalous heating phenomenon that can occur from the clash of mesh effects, geometric convergence, and Monte Carlo noise. We were able to successfully eliminate the abnormal heating, but only at the cost of decreased numerical accuracy.

The second method utilized a very efficient approach for obtaining a center value for the widely used Monte Carlo variance reduction method known as weight windows. With weight windows, particles whose weights are above the weight window are split into additional average-weight particles, and particles below the weight window undergo Russian Roulette to increase the computational efficiency. Our approach utilized the previous time step's intensity as the weight window center, resulting in a higher Monte Carlo efficiency for problems containing optically thick materials where the radiation intensity changes very slowly. Problems containing optically thin materials performed as expected and conditions were added to allow for increased Monte Carlo efficiency for problems containing a mix of thick and thin materials. However, we have recently discovered an issue that may

allow thermal energy to travel too far. Near the interfaces between thick and thin materials, our method introduces an unphysical heat up resulting in inaccurate material temperatures.

DEDICATION

To Bill Murray.

ACKNOWLEDGMENTS

This material is based upon work supported by the Department of Energy, National Nuclear Security Administration, under Award Number(s) DE-NA0002376.

I would like to thank the Nuclear Engineering department at Texas A&M University for all of the resources they have provided for me. Special thanks to Ryan G. McClarren for advising me throughout graduate school at Texas A&M University. Also, I would like to specially thank Nicholas Gentile for his mentorship during my time at Lawrence Livermore National Laboratory.

In addition, I would like to thank my office mates: Yuriy Ayzman, Simon Bolding, Kelli Humbird, Lance Merchant, Pablo Vaquer, and Rick Vega. I appreciate your patience with me when pestering you all with questions. I don't know if I would have survived the nuclear engineering graduate program without ya.

I would like to thank my family and friends for believing in me and always having my back. More importantly, I would like to thank CTG, Cody Cliffhanger, the Gutsy Dinosaur, and the Zachlar for the endless late night shenanigans, but hey, that's just life as it is.

Lastly, I would like to thank the gates of north. Without your succulent liquids, life in Aggieland wouldn't have been the same.

NOMENCLATURE

OGAPS	Office and Graduate and Professional Studies at Texas A&M University
TAMU	Texas A&M University
TRT	Thermal Radiative Transfer
GTRT	Gray Thermal Radiative Transfer
MC	Monte Carlo
IMC	Implicit Monte Carlo
FINMCOOL	Fully Implicit Non linear Monte Carlo Object-Oriented Language
LLNL	Lawrence Livermore National Laboratory
jk	jerk (unit of energy equivalent to 10^9 Joules)
sh	shake (unit of time equivalent to 10^{-8} seconds)
keV	kiloelectron-volt
pdf	probability density function

TABLE OF CONTENTS

Page

LIST OF FIGURES

FIGURE Page

1. INTRODUCTION

The emergence of modern supercomputers has led to an increase in the use of numerical simulations to reproduce full-scale scientific experiments. The accuracy of these simulations is typically constrained by problem inputs, and in the case of the Monte Carlo method, the number of particle histories simulated. However, within the scientific community, ongoing research is being conducted to develop methods which aim to decrease the uncertainty in numerical simulations without exhausting computational resources through dimensional refinement.

This thesis develops, tests, and analyzes two new methods for decreasing the variance associated with the Implicit Monte Carlo method, which is a stochastic radiation transport model commonly used to simulate inertial confinement fusion. The work contained in this thesis has been implemented and tested using FINMCOOL, which is an IMC code developed at Texas A&M University.

1.1 Implicit Monte Carlo

Long before the construction of the first computer, particle transport experiments were conducted using the Monte Carlo method [1]. This method is a stochastic numerical scheme, which relies on repeated random sampling to simulate how particles are transported through media. Random number generators are used to determine spatial locations for particle emission as well as directions of travel. In addition, this method takes advantage of the randomness of particle interactions to simulate how far particles will travel and what types of interaction they will undergo. Typically, particles can either exit the problem domain, be absorbed, or scatter, resulting in a new direction of travel. Particle "histories" are independently transported until they either reach the end of the time step or are terminated, through leakage or absorption.

The Monte Carlo method can easily model complex three-dimensional geometries, however, it can take long periods of time to yield meaningful results. While particles are being transported, quantities of interest, such as energy deposition, are accumulated and stored as tallies. Typically, the uncertainty of a Monte Carlo tally converges on the order of $1/\sqrt{N}$, where N is the number of particle histories being simulated. This slow convergence further indicates the need for variance reduction methods coupled with traditional Monte Carlo.

In 1971, Fleck and Cummings developed the means for handling the complexity of the coupled radiation transport equation and material energy equation [2]. This method, denoted Implicit Monte Carlo (IMC), simulates a photon's absorption/re-emission within a single time step via "effective" scattering, resulting in the need for considerably fewer time steps. The method is not actually derived using a truly implicit time discretization, but instead a semi-implicit treatment is performed. This treatment solves for the specific intensity via a standard linear Monte Carlo method and then updates the temperature at the end of a time step using the solution that was just computed. This allows the numerical scheme to remain unconditionally stable, without the need of performing a coupled nonlinear solve [3].

1.1.1 Thermal Radiative Transfer

The thermal radiative transfer (TRT) equations [4], which describe the scattering, and absorption of photons emitted from high-energy materials are given as:

$$\begin{aligned}\frac{1}{c}\frac{\partial I}{\partial t}(x,\mu,\nu,t) + \mu\frac{\partial I}{\partial x}(x,\mu,\nu,t) + \sigma_a(x,\nu,T)I(x,\mu,\nu,t) \\ = 2\pi\sigma_a(x,\nu,T)B(\nu,T) + \frac{Q}{2}(x,\nu,t),\end{aligned} \tag{1.1}$$

$$c_v(x,T)\frac{\partial T}{\partial t}(x,t) = \int_0^\infty \int_{-1}^1 \sigma_a(x,\nu',T)[I(x,\mu',\nu',t) - 2\pi B(\nu',T)]\, d\mu' d\nu', \quad (1.2)$$

where

$$I = chvn(x,\mu,\nu,t) = \text{the specific intensity}, \quad (1.3)$$

$$n(x,\mu,\nu,t) = \text{the mean number of photons per unit of phase space}, \quad (1.4)$$

$$h = 6.6260693 \times 10^{-35} \text{ jk-sh = Planck's constant}, \quad (1.5)$$

$$c = 299.792458 \text{ cm/sh = speed of light}, \quad (1.6)$$

$$T = T(x,t) = \text{material temperature (keV)}, \quad (1.7)$$

$$B = B(\nu,t) = \text{Planck's function for radiation}, \quad (1.8)$$

$$= \frac{2h\nu^3}{c^2}\left(e^{h\nu/T} - 1\right)^{-1}, \quad (1.9)$$

$$Q = Q(x,\nu,t) = \text{inhomogenous photon source}, \quad (1.10)$$

$$c_v = c_V(x,T) = \text{specific heat of material}, \quad (1.11)$$

$$\sigma_a = \sigma_a(x,\nu,T) = \text{the absorption opacity}, \quad (1.12)$$

$$= \text{probability of absorption per unit distance}. \quad (1.13)$$

All of the variables are known quantities except for the radiation intensity, I, and the material temperature, T. Additionally, it is appropriate to define the material and radiation

energy densities as follows:

$$\frac{\partial U_m}{\partial T}(x,t) = c_v(x,T) = \text{material energy density} \tag{1.14}$$

$$U_r(x,t) = aT(x,t)^4 = \text{radiation energy density} \tag{1.15}$$

where

$$a = \text{radiation constant} = \frac{8\pi^5 k^4}{15h^3c^3} = 0.01372\frac{\text{jk}}{\text{cm}^3\text{keV}^4}, \tag{1.16}$$

$$k = \text{Bolzmann's constant} = 1.60219e-31 \text{ Gj/keV}. \tag{1.17}$$

It is useful to understand the physical meanings of each of the terms within the TRT equations (Eq. (1.1) and Eq. (1.2)). The first term in Eq. (1.1) is the time rate of change term, which describes how the radiation Intensity changes due to several losses and gains. The second term describes how photons are lost from streaming out of the phase space. The third term is also a loss term, which physically describes how photons are absorbed within the background material. The first term on the right side of Eq. (1.1) is a gain term, which comes from a radiative source due to the temperature of the background material. The last term on the right hand side describes the presence of a physical source of radiation. Within the material energy equation, Eq. (1.2), we see a time rate of change term for the material energy density, which is described by the gain of energy through absorption of radiation, and loss of energy through emission. The two TRT equations are nonlinearly coupled by means of the material temperature, which further increases their complexity.

1.1.2 The Gray Approximation

The work presented in this thesis was performed for frequency-independent (gray) problems. This means that the material opacities are independent of the photon frequency,

which allows for simplifications to made to the TRT equations by integrating over all frequencies. We do this by defining:

$$I(x\mu, t) = \int_0^\infty I(x, \mu, \nu, t)\, d\nu, \tag{1.18}$$

$$Q(x, t) = \int_0^\infty Q(x, \nu, t)\, d\nu, \tag{1.19}$$

$$\frac{ac}{4\pi}T^4 = \int_0^\infty B(\nu, T)\, d\nu, \tag{1.20}$$

which allows us to rewrite the TRT equations as:

$$\begin{aligned}\frac{1}{c}\frac{\partial I}{\partial t}(x, \mu, t) + \mu\frac{\partial I}{\partial x}(x, \mu, t) + \sigma_a(x)I(x, \mu, t) \\ = \sigma_a(x)\frac{ac}{2}T^4(x, t) + \frac{Q}{2}(x, t),\end{aligned} \tag{1.21}$$

$$c_v(x, T)\frac{\partial T}{\partial t}(x, t) = \int_{-1}^{1} \sigma_a(x)[I(x, \mu', t) - \frac{ac}{2}T^4(x, t)]\, d\mu', \tag{1.22}$$

These equations are known as the Gray Thermal Radiative Transfer equations and are the equations we solve in this work.

1.1.3 Time Discretization and Linearization of the Transport Equation

Following Fleck and Cummings' derivation, we naturally start with the GTRT equations, recasted using the relationships defined in Eq. (1.14) and Eq. (1.15).

$$\frac{1}{c}\frac{\partial I}{\partial t} + \mu\frac{\partial I}{\partial x} + \sigma_a I = \frac{1}{2}\sigma_a c U_r + \frac{Q}{2}, \tag{1.23}$$

$$\frac{\partial U_m}{\partial t} = \sigma_a \left(\int_{-1}^{1} I \, d\mu - cU_r \right), \tag{1.24}$$

Note that we have suppressed the variable parameters for clarity. We define

$$\frac{\partial U_m}{\partial U_r} = \beta^{-1}, \tag{1.25}$$

so that we may write Eq. (1.24) as

$$\frac{\partial U_r}{\partial t} = \beta\sigma_a \left(\int_{-1}^{1} I \, d\mu - cU_r \right), \tag{1.26}$$

In the case that the background material is a perfect gas, meaning the specific heat is constant, the material energy can be defined as $U_m = bt$, where b is a variable independent of temperature. This allows β to become

$$\beta = \frac{\partial U_r}{\partial U_m} = \frac{4aT^3}{b} = \frac{4U_r}{U_m}. \tag{1.27}$$

We then integrate Eq. (1.26) from time t^n to t^{n+1} and obtain the following result:

$$U_r^{n+1} - U_r^n = \int_{t^n}^{t^{n+1}} dt\beta\sigma_a \int_{-1}^{1} I d\mu - c \int_{t^n}^{t^{n+1}} dt\beta\sigma_a U_r, \tag{1.28}$$

where the superscript n denotes a variable at time t^n and the superscript $n+1$ denotes a variable at time t^{n+1}. At this point, Fleck and Cummings rewrote Eq. (1.28) using appropriate average values for the integrands as follows:

$$U_r^{n+1} - U_r^n = \Delta t \bar{\beta}\bar{\sigma}_a \left\{ \int_{-1}^{1} \bar{I} d\mu - c \left[\alpha U_r^{n+1} + (1-\alpha) U_r^n \right] \right\}, \tag{1.29}$$

where α is an unspecified coefficient that defines the time centering of the mean value of the radiative energy density. We then solve for U_r^{n+1} and obtain

$$U_r^{n+1} = \left[\frac{1-(1-\alpha)\bar{\beta}c\Delta t\bar{\sigma}}{1+\alpha\bar{\beta}c\Delta t\bar{\sigma}}\right]U_r^n + \frac{\bar{\beta}\bar{\sigma}\Delta t}{1+\alpha\bar{\beta}c\Delta t\bar{\sigma}}\int_{-1}^{1}\bar{I}d\mu \tag{1.30}$$

By rearranging, we can solve for the desired time averaged value of the radiation energy density, which simplifies to

$$\bar{U}_r = \alpha U_r^{n+1} + (1-\alpha)U_r^n \tag{1.31}$$

$$= \frac{\alpha\bar{\beta}\bar{\sigma}\Delta t}{1+\alpha\bar{\beta}c\Delta t\bar{\sigma}}\int_{-1}^{1}\bar{I}d\mu + \frac{U_r^n}{1+\alpha\bar{\beta}c\Delta t\bar{\sigma}}. \tag{1.32}$$

Here, it is common to introduce a term denoted the "Fleck Factor", which is defined as

$$f = \frac{1}{1+\alpha\bar{\beta}c\Delta t\bar{\sigma}}. \tag{1.33}$$

By substituting the Fleck Factor into Eq. (1.32), we can further simplify the definition of the time averaged radiative energy density to

$$\bar{U}_r = \alpha\bar{\beta}\bar{\sigma}\Delta t f\int_{-1}^{1}\bar{I}d\mu + U_r^n f. \tag{1.34}$$

Now, we substitute the definition of $\bar{U}_r$ into the transport Eq. (1.23) and substitute the instantaneous value of I for $\bar{I}$ to obtain

$$\begin{aligned}\frac{1}{c}\frac{\partial I}{\partial t} + \mu\frac{\partial I}{\partial x} + \sigma I - \frac{Q}{2} &= \frac{1}{2}\sigma c\bar{U}_r \\ &= \frac{1}{2}\sigma\alpha\beta c\Delta t\sigma f\int_{-1}^{1}Id\mu + \frac{1}{2}c\sigma U_r^n f\end{aligned} \tag{1.35}$$

Here, Fleck and Cummings define two contributions to the total cross section, the effective absorption cross section, σ_a, and the effective scattering cross section, σ_s, as follows:

$$\sigma_a = \frac{1}{1 + \alpha\beta c\Delta t\sigma}\sigma = f\sigma, \tag{1.36}$$

$$\sigma_s = \frac{\alpha\beta c\Delta t\sigma}{1 + \alpha\beta c\Delta t\sigma}\sigma = (1 - f)\sigma, \tag{1.37}$$

Previously, the system may or may not have had real scattering, however, now the system will have an added effective scattering term. The Fleck factor prescribes how much the absorptions/re-emission process is approximated by effective scattering. It is understood that as the time step becomes large, the fleck factor approaches zero, increasing the dominance of the effective scattering process. This implies that during larger time steps, there is an increased likelihood that absorbed particles will become re-emitted, which is physically true. This behavior was intentionally designed in order to reduce the computational expenses associated with having to simulate many absorptions and re-emissions. With these definitions, Fleck and Cummings go on to show that the transport equation in the form (1.35), passes a slew of consistency tests, proving that solving the derived equation leads to self-consistent numerical solutions that satisfy the basic GTRT equations (1.23) and (1.24) [2]. Furthermore, the scheme for updating the material energy density is obtained by first integrating Eq. (1.35) over all directions, obtaining

$$\frac{\partial U_m}{\partial t} = \frac{\sigma}{1 + \alpha\beta\sigma c\Delta t}\int_{-1}^{1} I\, d\mu - \frac{c\sigma U_r^n}{1 + \alpha\beta c\Delta t\sigma} + \frac{Q}{1 + \alpha\beta c\Delta t\sigma}. \tag{1.38}$$

Physically, the first term on the right side of Eq. (1.38) represents the material heating rate due to effective absorptions. The other two terms represent the emission from the background material and the heating rate of the physical source. Integrating this Eq. (1.38)

between t^n and t^{n+1}, results in

$$U_m^{n+1} = U_m^n + \frac{\sigma}{1+\alpha\beta c\Delta t\sigma}\int_{t^n}^{t^{n+1}} dt \int_{-1}^{1} I\, d\mu - \frac{c\Delta t\sigma U_r^n}{1+\alpha\beta c\Delta t\sigma} + \frac{Q\Delta t}{1+\alpha\beta c\Delta t\sigma}, \quad (1.39)$$

which under the perfect gas assumptions ($U_m = bT$), becomes

$$T^{n+1} = T^n + b^{-1}\left\{\frac{\sigma}{1+\alpha\beta c\Delta t\sigma}\int_{t^n}^{t^{n+1}} dt \int_{-1}^{1} I\, d\mu - \frac{c\Delta t\sigma U_r^n}{1+\alpha\beta c\Delta t\sigma} + \frac{Q\Delta t}{1+\alpha\beta c\Delta t\sigma}\right\}, \quad (1.40)$$

In the case of a non-perfect gas, one may substitute $\partial U_m/\partial T$ in place of b. Analytically, Eq. (1.35) is not solvable. Instead, we must solve this equation numerically by means of Monte Carlo or a deterministic solver.

1.1.4 The Implicit Monte Carlo Procedure

In a Monte Carlo simulation, particles are randomly sampled and transported using constructed probability density functions, which describe the physical events a particle can undergo. Usually, many such particles are samples and their events are tallied and averaged using a weighting factor unique to each particle. Typically, the particle "weight", w_0, is a dimensionless quantity that can be interpreted as the relative number of neutrons represented by a Monte Carlo particle. In an IMC simulation, however, the particle weight describes the amount of energy that is represented by a single Monte Carlo particle and is often denoted an "energy-weight". Thus, in an IMC simulation, particle energies are transported through the system until said energy either leaks out of the system, is absorbed by the background material, or reaches the end of a time step.

The energy-weights of each IMC particle is calculated at the beginning of the simulation and the beginning of each subsequent time step. Typically, the number of desired particle histories is specified and then divided among each of the possible energy sources contained within the system. For instance, in the first time step, photons may represent

the energy from the initial condition, the boundary condition, a physical source, or the material, if the temperature is greater than zero. For an individual source, the number of particle histories, N_i would be equal to

$$N_i = \frac{\text{Energy of source } i}{\text{Total energy within the system}}. \tag{1.41}$$

Naturally, the energy-weight of each particle within source, i, would be equal to

$$w_{0,i} = \frac{\text{Energy of source } i}{N_i}. \tag{1.42}$$

Each particle location and angle is then randomly sampled (usually uniformly). In addition, the emission times of the photons representing the material temperature are sampled uniformly throughout the current time step.

After all of the particles have been created, they are individually transported, undergoing one of three events: the particle collision with an atom, exiting the current zone, reaching the end of the time step, t_{n+1}. Each of the three possible outcomes will have an associated distance: a distance to collision, a distance to a spatial boundary, and the distance traveled until the photon's time is equal to t_{n+1}. The distance to the boundary (for a simplified 1-D slab geometry), d_b, is equal to

$$d_b = \frac{x_b - x}{\mu}, \tag{1.43}$$

where μ is the particle direction toward boundary, x_b , and, x is the particle location before transporting. The distance traveled until t_{n+1}, d_t, is

$$d_t = c(t_{n+1} - t), \tag{1.44}$$

where t is the time before transporting the particle. In a typical Monte Carlo simulation, the distance to the next collision event is obtained by inverting the probability density function for removals due to collisions. However, in IMC, it is common to use a technique known as "Implicit Capture", in which a particle's energy is continuously absorbed as it travels. This technique is discussed to a greater extent in the next section, however is necessary to mention because it affects the tracking procedure. With implicit capture, one entirely removes absorption "events" and replaces the distance-to-collision, with a distance-to-scatter. Thus the distance-to-scatter, d_s is obtained by inverting the pdf for removals due to scattering as follows

$$d_s = \frac{\ln(\xi)}{\sigma_s}, \tag{1.45}$$

where ξ is a random number uniformly sampled on [0,1], and σ_s is the scattering opacity. The minimum distance, s, determines which of the three events will occur. If the photon reaches the end of the time step, it is placed into the "census" where it will remain until the tracking procedure is continued in the next time step. If the photon reaches a boundary, the particle can either (1) exit the system or (2) enter a new zone, where it will continue to be tracked until being terminated or reaching t_{n+1}. If the photons undergoes a scatter event, the particle's direction will change and the tracking procedure will proceed. During each event, the particle's energy-weight is exponentially attenuated (due to implicit capture) as follows:

$$w_p = w_0 e^{-s\sigma f}. \tag{1.46}$$

Additionally, the energy absorbed into the material is accumulated in order to determine the material temperature at the end of the time step (which quantifies the amount of energy

emitted in the next time step), Furthermore, the particle intensity, I, is tallied as follows:

$$I = \frac{w_0}{\sigma f}\left(1 - e^{-s\sigma f}\right). \tag{1.47}$$

1.2 Variance Reduction Strategies

Due to the stochastic nature of Monte Carlo simulations, there will be some associated uncertainty in the solutions obtained from an IMC simulation. The IMC method has proven to significantly improve the accuracy and stability of radiation transport simulations, however, insufficient computational resources combined with adverse problem characteristics can still lead to unphysical results and anomalies. Thus, in an attempt to increase the confidence in the solution, we often modify the Monte Carlo procedure using, what we refer to as, variance reduction methods.

The convergence rate of a Monte Carlo simulation, $0(N^{-1/2})$, is independent of dimension, which makes it a viable method for high-dimensional problems. However, the rate $0(N^{-1/2})$ is decelerating, since additional increases in computational effort provide fractional improvement in accuracy, which further indicates the need for strategies that accelerate this convergence. The variance reduction methods we explore aim to "accelerate the convergence rate by reducing the constant in front of the $0(N^{-1/2})$" [5].

1.2.1 Implicit Capture

During an IMC simulation, it is typical to use implicit capture to reduce the variance associated with energy deposition. During implicit capture, a particle is continuously absorbed as it streams by removing the absorbed energy from the particle's weight and adding it into the background material. With this technique, absorption "events" are removed entirely from the tracking procedure, resulting in the need of a distance to a scattering event opposed to a distance to collision. Prior to scattering, a particle's energy is

exponentially attenuated throughout its flight.

1.2.2 Splitting and Russian Roulette

Particle splitting and Russian Roulette typically go hand in hand when implemented within the Monte Carlo procedure. The basic idea is to effectively create average-energy-weight particles throughout the system. Low-energy-weight particles will typically undergo Russian Roulette during transportation, ridding the system from particles that do not significantly contribute to the solution, by effectively combining low-energy-weight particles into a single, average-energy-weight particle. On the contrary, splitting turns a single high-energy-weight particle into a legion of identical average-energy-weight particles.

1.2.3 Volume-Dependent Fleck Factor

Recent discoveries have shed light on a particular issue caused by the interaction of Monte Carlo noise and mesh effects in problems that have very large changes in zone volume, such as in RZ geometry. In such a situation, it is possible for "anomalous heating" to occur when using IMC in combination with implicit capture. We have found that if a single particle were to stream through multiple zones, unphysical heating could occur if the energy deposited in one zone was less than the energy deposited in all subsequent zones i.e.

$$\frac{E_i}{V_i} < \frac{E_{i+1}}{V_{i+1}} \tag{1.48}$$

Here the indexes i and $i+1$ correspond to a particle's current and next zone, E_i is the energy absorbed by the material in zone i, and V_i is the volume of zone i. Due to this effect, we proposed adding a volumetric dependence to the Fleck factor, which would have a diminishing effect, implying that the particle is more likely to be absorbed and re-emitted within a given time step.

1.2.4 Weight Windows

Weight windows are widely used for variance reduction in Monte Carlo simulations [6, 7, 8, 4, 9]. When using this technique, each cell in a mesh is given a weight window center, which is bounded by higher and lower values. As particles enter into new cells, a check will be performed to determine whether or not each particle's "weight" (energy for IMC) is within the weight window. Particles whose weights are above the weight window will be split into additional particles, and particles whose weights are below the weight window will undergo some other technique, such as Russian Roulette [10, 11], to remove the particle from the simulation, increasing the computational efficiency. We utilized Russian Roulette for most of our simulations, which effectively combine several low-weight particles into one.

"Establishing a procedure that produces a nearly optimal weight window center for IMC transport problems remains an open question"[3]. In 2009, Becker and Larsen came up with a way to analyze how different weight windows approaches would perform on particular problems [8] by developing a formulation to analyze a specific weight window center. Wollaber [4] used the solution of a quasi-diffusion problem to select the weight window center for IMC solutions to radiative transfer problems. In our work, we decided to take a much simpler approach by analyzing the effects from using a "lagged" weight window center, meaning we used the solution from a previous time step to set the weight window center.

2. USE OF A VOLUME-DEPENDENT FLECK FACTOR FOR ADDED ROBUSTNESS

Towards the end of the previous chapter, we mentioned that it is possible for anomalous heating to occur in problems that have very large changes in zone volumes. It is typical to use implicit capture to reduce the energy deposition variance of IMC simulations. However, when too few of particles are used within a simulation, a particle may deposit more energy within smaller volume zones due to the clash of mesh effects, geometric convergence and Monte Carlo noise. To address this issue, we have added a volume-dependence to the Fleck factor to decrease the Fleck factor where the zone volume is the smallest, effectively removing anomalous heating on the axis [12].

2.1 Conditions for Anomalous Heating

To derive the condition for which anomalous heating can occur, we consider an instance of a particle traveling in an axisymmetric, RZ geometry toward the axis. In such a mesh, as the particle travels, the zone volumes the particle passes through will be decreasing. If the material is optically thin, it is possible that in two different zones the particle will deposit similar amounts of energy. However, due to the volume change, the actual heating in the smaller zone will be higher (because the temperature in the zone is related to the internal energy density). This type of heating caused by volumetric changes in the mesh, we call anomalous heating.

To better quantify this effect, we consider a hypothetical mesh comprised of three zones of equal width, but decreasing in volume. We examine the case in which a single particle enters the largest zone, and then travels through all three zones without undergoing a scattering event. Due to implicit capture, the material will continuously absorb energy

as the particle streams. This is energy is defined as:

$$E_i = f_i \sigma_i w_i \int_0^{S_i} e^{-f_i \sigma_i s} ds, \tag{2.1}$$

where f_i is the Fleck factor [2], σ_i is the material opacity, w_i is the initial energy-weight of the particle as it enters zone i, and S_i is the step length of the particle. The exact solution of this integral equates to:

$$E_i = w_i \left(1 - e^{-f_i \sigma_i S_i}\right). \tag{2.2}$$

If we instead simplify this integral by using a two-term power series approximation for the exponential term, we obtain:

$$E_i \approx w_i f_i \sigma_i S_i. \tag{2.3}$$

Ignoring energy radiated from these zones, the change in material energy due to the single particle is:

$$\Delta E_i = \frac{E_i}{V_i}, \tag{2.4}$$

where V_i is the volume of zone i. It is understood that anomalous heating can occur if the change in material energy density in the first zone was less than the change in material energy in subsequent zones (i.e. $\Delta E_i < \Delta E_{i+1}$). Equation (2.4) is substituted into this inequality to derive the condition in which anomalous heating could occur.

$$\frac{E_i}{V_i} < \frac{E_{i+1}}{V_{i+1}} \tag{2.5}$$

Substituting Eq. (2.3) result in:

$$\frac{w_i f_i \sigma_i S_i}{V_i} < \frac{w_{i+1} f_{i+1} \sigma_{i+1} S_{i+1}}{V_{i+1}}, \tag{2.6}$$

which simplifies to:

$$V_{i+1} < \left(\frac{w_{i+1} f_{i+1} \sigma_{i+1}}{w_i f_i \sigma_i} \right) V_i. \tag{2.7}$$

This condition quantifies the relationship in mesh-cell volumes that allows anomalous heating to occur. It also indicates how we can use the change in volume to avoid such anomalous heating in a problem consisting of zones with varying volumes (e.g., RZ or AMR meshes).

2.2 Addition of the Volume-Dependent Fleck Factor

To prevent the heating abnormality, a volume-dependent Fleck factor is proposed, so that the Fleck factor is now defined as:

$$f \rightarrow \left(\frac{V_i}{V_\varnothing} \right) f, \tag{2.8}$$

under the condition that:

$$V_i < \left(\frac{w_i f_i \sigma_i}{w_\varnothing f_\varnothing \sigma_\varnothing} \right) V_\varnothing, \tag{2.9}$$

where $\varnothing$ is the zone the particle was born in. In effect, this change in the Fleck factor decreases the Fleck factor when the particle enters a zone of smaller volume than the one it was born in. Considering the same hypothetical mesh, and performing similar derivations as seen in the previous section, the energy absorbed within each zone can now be approximated as:

$$E_i \approx w_i \frac{V_i}{V_\varnothing} f_i \sigma_i S_i. \tag{2.10}$$

Once again the case in which $\Delta E_i < \Delta E_{i+1}$ is considered. Substituting Eqs. (2.4) and (2.10) into the inequality results in:

$$\frac{w_i f_i \sigma_i S_i}{V_\varnothing} < \frac{w_{i+1} f_{i+1} \sigma_{i+1} S_{i+1}}{V_\varnothing}, \tag{2.11}$$

which simplifies to:

$$w_i f_i \sigma_i S_i < w_{i+1} f_{i+1} \sigma_{i+1} S_{i+1}. \tag{2.12}$$

Though it is not very likely, Eq. (2.12) reveals that it is still possible for anomalous heating to occur. However, we have shown that the addition of a volume-dependent Fleck factor will prevent these abnormalities due primarily to differences in zone volumes.

2.3 Test Problem

To demonstrate both the problem of anomalous heating and the benefits of the volume-dependent Fleck factor, we devised a problem according to the following heuristic: we wanted an RZ problem where a strong source at a large radius emitted photons that would reach the axis at a grazing angle. Such a problem would have few particles reaching the axis, but those that did would carry a significant amount of energy. The problem configuration we settled on is shown in Fig. 2.1.

This problem consists of three different materials, which can be identified by the labels 5, 50, and 501, which were all user specified labels. The three materials have opacities equal to $\sigma = 1$ cm^{-1}, $\sigma = 300T^{-3}$ cm^{-1}, and $\sigma = 3T^{-3}$ cm^{-1}, respectively, with T in keV. Each has a constant heat capacity given by $C_{\mathrm{v}} = 0.01$, 0.3, and 0.01 GJ/cm^3/keV, respectively. The initial temperature is set to 0.001 keV with a boundary source at 300 eV on the left side of the top left region. The simulations shown in this work used 10^4 particles per time step. In our figures, the "x" axis depicts the z direction while the "y" axis depicts the radial direction. The line extending across region 5 depicts the location of a line-out, which is used for convergence analysis in a later section.

The problem was run using the FINMCOOL code developed at Texas A&M and we present results for the material temperature and standard deviation of the material temperature. We also present a higher resolution solution using 3×10^6 particles per time step, which allows us to estimate the accuracy of our simulations.

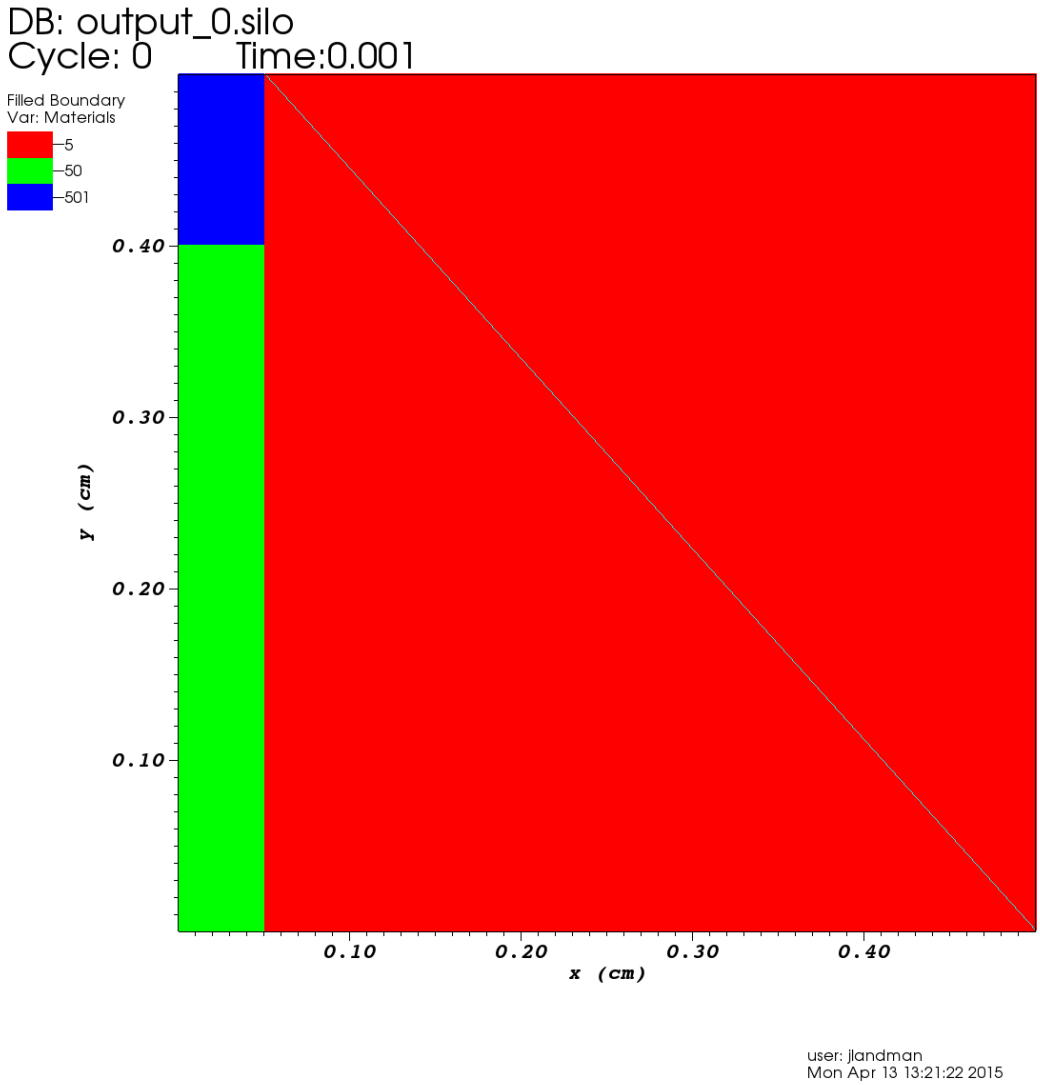

Figure 2.1: RZ problem configuration. There is a 300 eV blackbody source at the left of material 501. In this and the next two figures the "x" axis depicts the z direction while the "y" axis depicts the radial direction.

2.4 Preliminary Results

Based off of prior theory, we expect to see anomalous heating as the y axis approaches zero where there are large decreases in zone volumes. The way this problem is set up, material 501 will heat up quickly and radiate energy into materials 50 and 5. Material 50 is

optically thick and cold, and material 5 is not optically thick. In the problem configuration all radiation from the source traveling directly toward the axis is blocked by material 50.

Figure 2.2 depicts the material temperature at $t = 5.37637$ ns. As expected, the figure illustrates the occurrences of abnormal heating in various zones near $r = 0$ where the difference in zone volumes is very large. In particular we notice that in the lowest in r zones there is a large amount of noise in the solution. We wish to mitigate this effect and prevent this unphysical phenomena with the use of a volume-dependent Fleck factor.

Figure 2.3 depicts the material temperature at $t = 5.37637$ ns with the use of a volume-dependent Fleck factor. During the simulation, the volume of the zone that birthed a given photon was stored in memory allowing the Fleck factor to be scaled by the ratio between the photon's current zone volume and the photon's initial zone volume, as indicated in Eq. (2.8). As anticipated, the volume-dependent Fleck factor was able to prevent anomalous heating due to the large changes in zone volumes.

To form an approximation of the statistical uncertainties associated with our numerical calculations, we executed 10 simulations with varying random seeds and determined standard deviations at each spatial location of the mesh. The benefits of the volume-dependent Fleck factor can be further seen in the standard deviation of the material temperature between the 10 independently-seeded calculations. The standard deviation of the material temperatures at $t = 5.37637$ ns is shown in Fig. 2.4 with a standard Fleck factor, and in Fig. 2.5 for results with a volume-dependent Fleck factor.

In these figures it is apparent that using the volume-dependent Fleck factor results in a much smaller standard deviation in the material temperature. The standard calculation has a standard deviation as high as 0.04 keV, about 10% of the maximum temperature in the problem. Additionally, near the axis the volume-dependent Fleck factor calculation has a smaller standard deviation in each zone. We note that the solution time for each of these calculations was basically the same, indicating that this reduction in noise was not at the

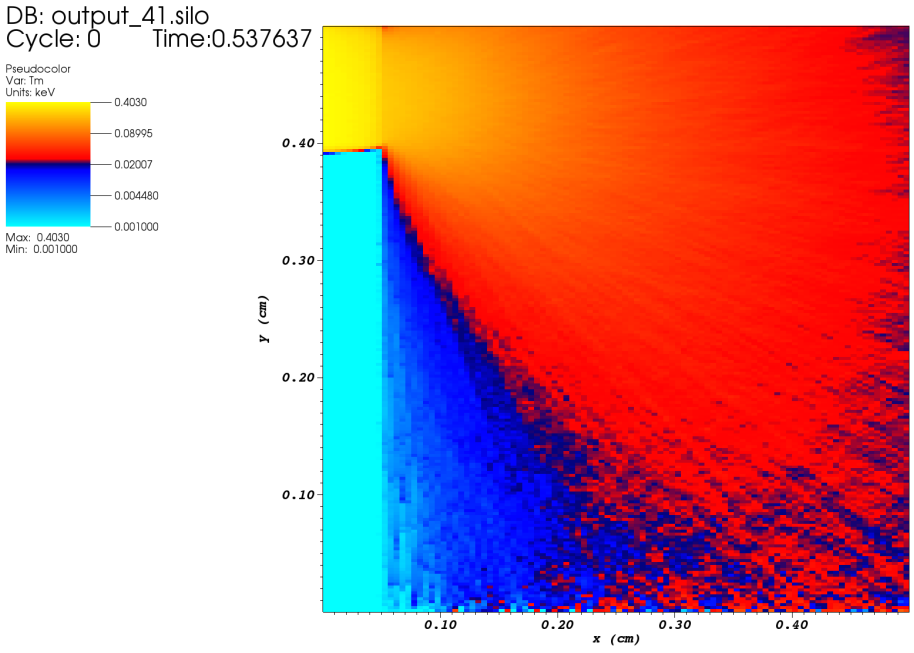

Figure 2.2: Material temperature at about 5.37 ns without using the volume-dependent Fleck factor. Note the logarithmic scale and the hot-cold color bar scheme.

cost of longer simulation times.

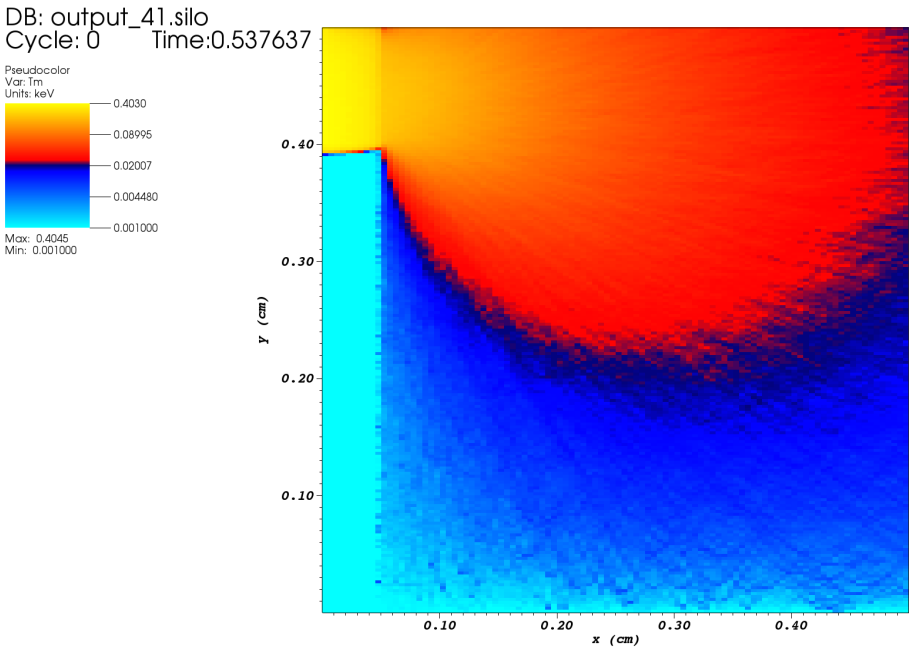

Figure 2.3: Material temperature at about 5.37 ns using the volume-dependent Fleck factor. Note the logarithmic scale and the hot-cold color bar scheme.

As a further comparison, we will look at a line out at $r = 0$ for both the material temperature and the standard deviation of the material temperature. In Fig. 2.6 the material temperature at $r = 0$ is shown. From this figure we see that the nominal value of the material temperature is lower for the volume-dependent Fleck factor results. Nevertheless, the amount that it is lower is small on an absolute scale. The standard Fleck factor solution in Fig. 2.6 appears noisy, and the standard deviation of the material temperature, shown in Fig. 2.7 bears this out. The standard deviation of the standard Fleck factor solution is about 2 orders of magnitude higher than the volume-dependent Fleck factor solution. Indeed, the standard method gives a standard deviation that is close to 100% of the actual material temperature shown in Fig. 2.6.

The introduction of the volume-dependent Fleck factor leads to smoother solutions by sacrificing the correct amount of absorption. We have effectively changed the physics of

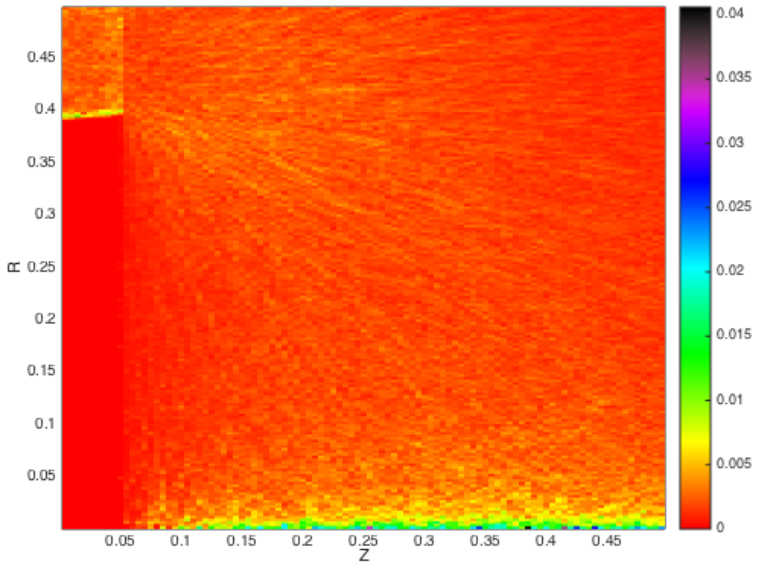

Figure 2.4: Standard deviation of the material temperature at about 5.37 ns without using the volume-dependent Fleck factor.

the problem in order to reduce the statistical noise in our simulations, which raises concerns regarding the introduction of a possible bias that could lead to a decrease in accuracy. In Fig. 2.8 a higher resolution solution for the material temperature is shown. We reiterate that the volume-dependent Fleck factor has shown to result in smoother simulations at the cost of an increase in actual error. This is better illustrated in Fig. 2.9 and Fig. 2.10, which show the average absolute difference, with and without the volume-dependent Fleck factor, between the 10 independently-seeded calculations and the high resolution solution. With the help of the volume-dependent Fleck factor, the magnitude of the absolute difference decreased, however, the amount of error increased.

2.5 Added Condition for Obtaining Correct Convergence

The addition of a Fleck factor that is dependent of the zone volume can ameliorate the negative effects of large changes in mesh volume. We were able to reduce noise in small

volume zones in an RZ calculation and avoid the anomalous heating that can occur when particles move across a mesh that has large changes in zone volume. In our numerical results, the prediction of anomalous heating was verified and our formulation of a volume-dependent Fleck factor performed as expected. However, our addition of the volume-dependent Fleck factor introduced a bias, which resulted in a decrease of accuracy. For some radiation transport problems in which you cannot use enough particles, opting for a smoother solution at the cost of accuracy may be ideal. Thus, it is necessary to formulate a way to control any biases such that the increase in error is much less than the expected statistical noise without using this approach.

Previously, the solution would not converge to the correct numerical solution as the number of IMC particles increased. To rectify this, we have added an additional condition, which allows the use of the volume-dependent Fleck factor if the number of particles

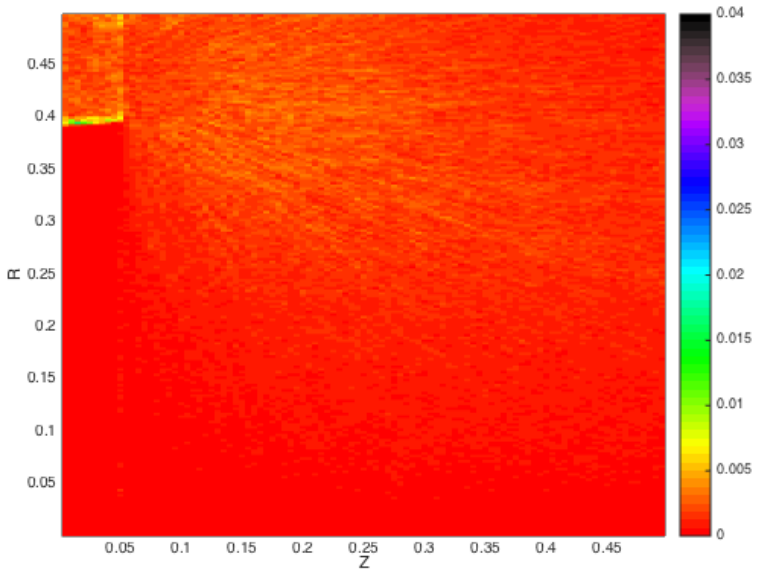

Figure 2.5: Standard deviation of the material temperature at about 5.37 ns using the volume-dependent Fleck factor.

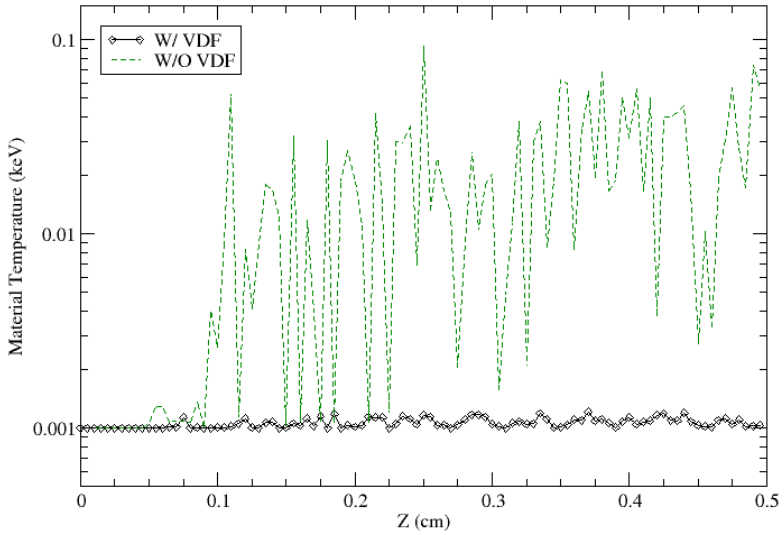

Figure 2.6: Material temperature at $r = 0$ at about 5.37 ns for the standard and modified methods. Note the logarithmic scale on the y-axis.

entering a particular zone is below a user specified number. For our analysis, we allowed the use of the volume-dependent Fleck factor if the number of particles entering into a zone was less than 50.

Figure 2.11 displays a line-out of the material temperature along the line displayed within Fig. 2.1. The figure contains plots for 6 different cases: two without the volume-dependent Fleck factor, and four with. Of the four plots that are using the volume-dependent Fleck factor, one does not use the new added condition, and three use the new condition. The number of desired particles used per time-step is displayed in parenthesis. Figure 2.11 shows that with the added condition, the solution will now converge to the correct numerical solution as the number of particle histories increases. However, for this particular problem, even when using 3×10^6 particles, the solution is not correct near the

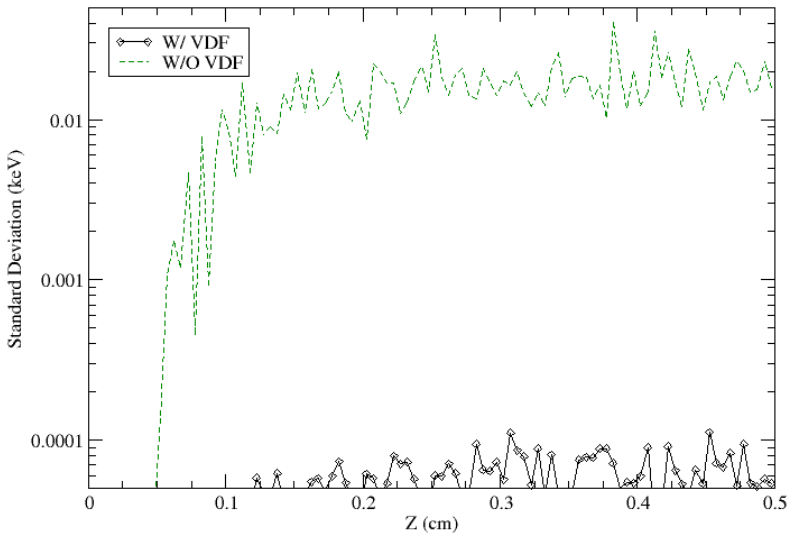

Figure 2.7: Standard deviation of the material temperature at $r = 0$ at about 5.37 ns for the standard and modified methods. Note the logarithmic scale on the y-axis.

end of the line-out. This is due to a lack of particles traveling the full extent of the mesh. Figure 2.12 depicts a binary comparison between (1) the absolute error, ϵ, associated with using a volume-dependent Fleck factor and (2) the expected statistical noise, κ, without using this approach. A value of 1 means that

$$\epsilon < \kappa, \tag{2.13}$$

while a value of 0 means the opposite. This figure illustrates that near the r = 0 axis, the resulting decrease in solution accuracy remains larger than the statistical noise without this method. Though the added condition results in correct convergence, it fails to mend the original issue, resulting in a large reduction in numerical accuracy. We do believe that our formulation for a volume-dependent Fleck factor can be a useful addition to IMC

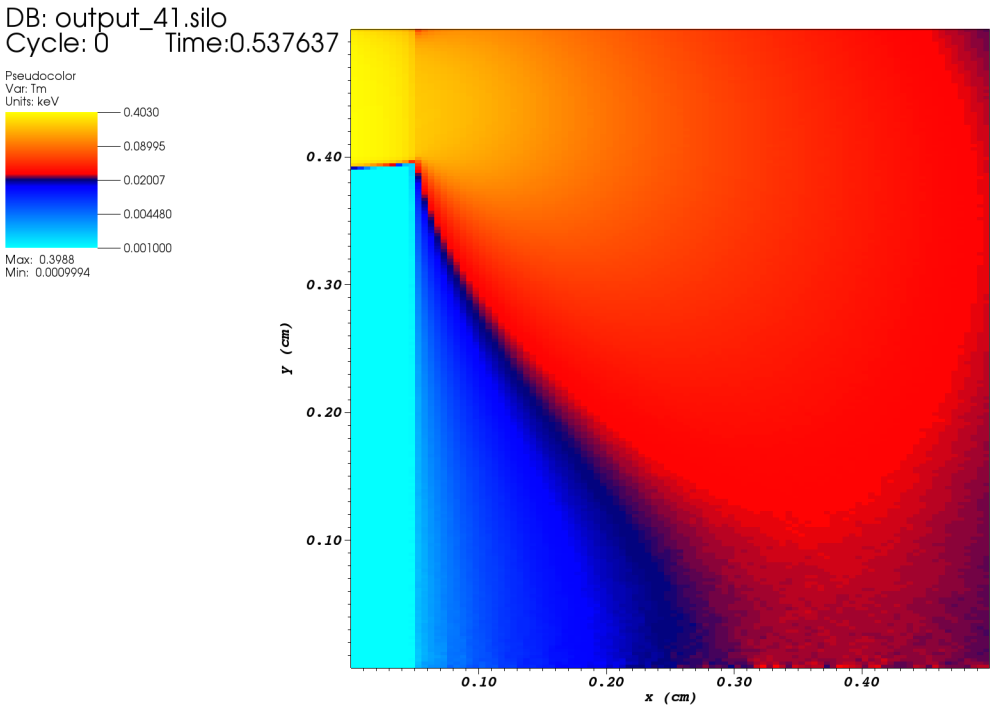

Figure 2.8: High resolution solution of the material temperature at about 5.37 ns without using the volume-dependent Fleck factor. Note the logarithmic scale and the hot-cold color bar scheme.

simulations with large changes in zone volume, however, the current state of the method is not yet well-equipped for wide use. Imposing a limit to the reduction of the Fleck factor may yield improved results, however, this has not been investigated.

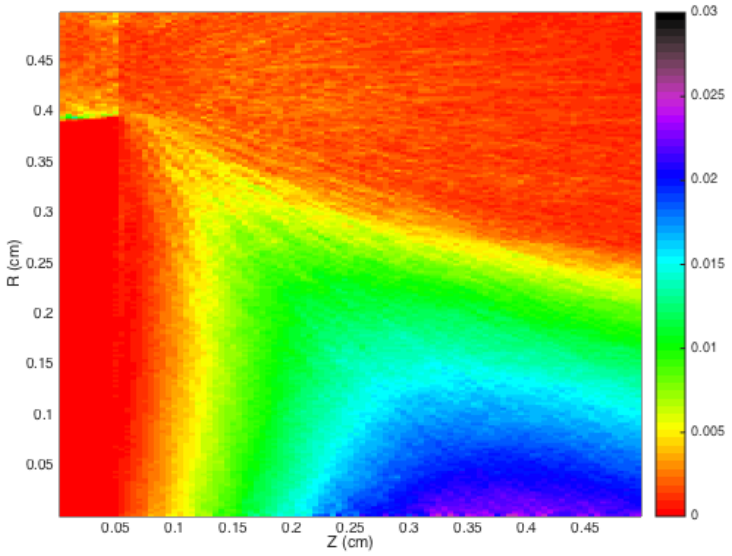

Figure 2.9: Average absolute difference between the 10 independently-seeded calculations ran with the volume-dependent Fleck factor and the higher resolution solution obtained using 300 times as many particles. Note that the maximum error is 0.0252.

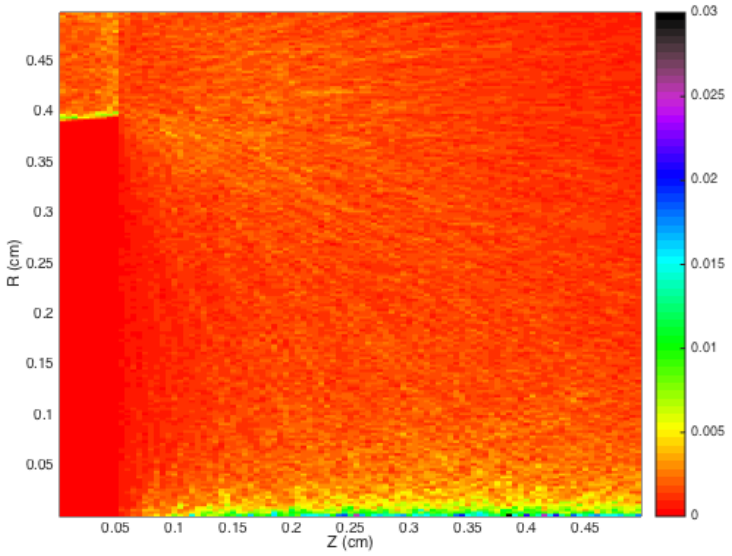

Figure 2.10: Average absolute difference between the 10 independently-seeded calculations ran without the volume-dependent Fleck factor and the higher resolution solution obtained using 300 times as many particles. Note that the maximum error is 0.0301.

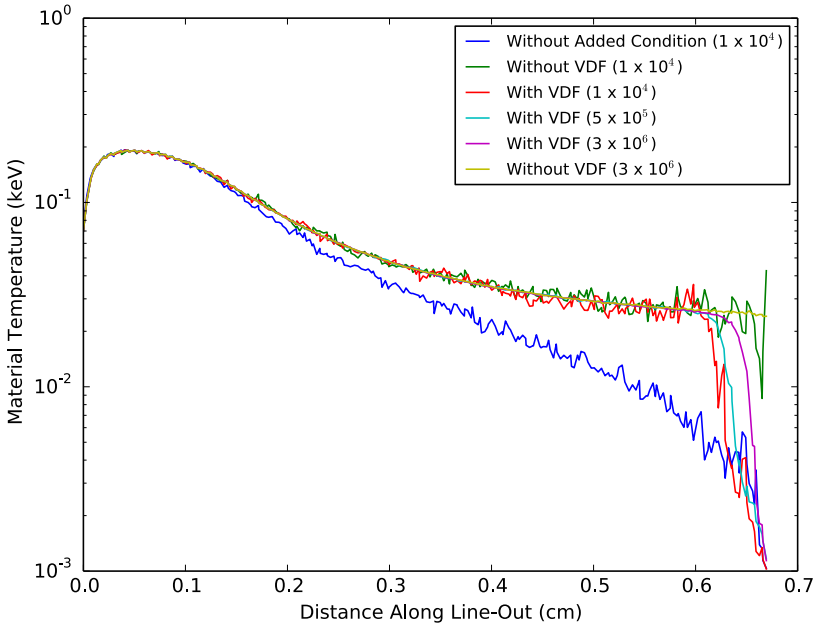

Figure 2.11: Material temperature along the line-out displayed in Fig. 2.1.

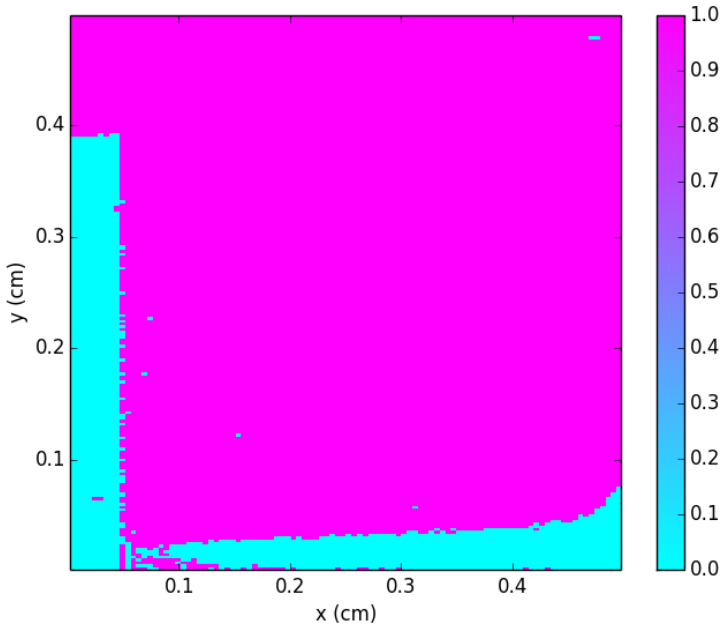

Figure 2.12: binary comparison between (1) the absolute error, ϵ associated with using a volume-dependent Fleck factor and (2) the expected statistical noise, κ. A value of 1 means that $\epsilon < \kappa$.

3. ANALYSIS OF A LAGGED WEIGHT WINDOW CENTER FOR VARIANCE REDUCTION [1]

3.1 Creating a Uniform Monte Carlo Particle Flux

A particular objective of weight windows is to increase the number of contributing particles to specific regions that contain low responses, allowing for more accurate and detailed information. Recent work by Becker and Larsen [8] developed a theory to analyze how different weight windows approaches will perform on a particular problem. In particular they studied the the Global Flux Weight Windows (GFWW) approach and the Forward-Weighted Consistent Adjoint-Driven Importance Sampling (FW-CADIS) approach. Their work showed that the following expression can be used to analyze the impact of the specified weight window center, $w(x, E)$, throughout space and energy,

$$\phi(\mathrm{x}, E) = Cw(x, E)M(x, E). \tag{3.1}$$

Here, $\phi(x, E)$ is the scalar flux and $M(x, E)$ is the theoretical Monte Carlo particle flux, and C is a constant that is typically 1. For problems where one is interested in the solution everywhere, it is usually desirable that $M(x, E)$ is as uniform as possible. Different methods select $w(x, E)$ differently and this has implications for the uniformity of $M(x, E)$. Wollaber [4] used the solution of a quasi-diffusion problem to select the weight window center for implicit Monte Carlo [2] solutions to radiative transfer problems. In that work he demonstrated a large degree of success on difficult Marshak wave problems.

In this work, we take a simpler approach that has the benefit of a nearly free improve-

[1] Reprinted with permission from "Analysis of Lagged Weight Windows for Implicit Monte Carlo Variance Reduction", by Jacob Landman et al., Published in Transactions, Vol. 111, pgs. 648-650, Winter 2014 meeting, Anaheim, CA, November 9-13, 2014, Copyright 2014 by the American Nuclear Society, LaGrange Park, Illinois.

ment in solution statistics [13]. For a given time step in an IMC calculation we use the previous time step's estimate of the scalar flux for the weight window center,

$$w(x, E) = \phi^{i-1}(x, E), \tag{3.2}$$

where the superscript $i - 1$ indicates the scalar flux is evaluated at the previous time step. The results we present here are only for gray (frequency-integrated) problems, so there is no energy dependence. Using Eq. (3.2) in Eq. (3.1), the theoretical particle flux can be shown to be

$$M(\mathrm{x}, E) = \frac{\phi(\mathrm{x}, E)}{C\phi^{i-1}(\mathrm{x}, E)} \tag{3.3}$$

In problems that are optically thick, one would expect that the scalar flux would be slowly changing as a function of time, therefore between time steps the ratio ϕ/ϕ^{i-1} should be close to unity throughout the problem, and $M(x, E)$ would be uniform. In problems with optically thin regions, and therefore large amounts of streaming, the ratio could be very large near a wavefront where $\phi \gg \phi^{i-1}$. Indeed, we see both of these phenomena in real simulations. In particular in a common Marshak wave problem [14], we see this lagged weight window center is quite effective, whereas in a 2-D cartesian version of the crooked pipe problem developed by Graziani and Leblanc [15], the streaming regions show issues with this method of selecting the weight window center.

3.1.1 1-D Marshak Wave Test Problem

A 1-D Marshak wave simulation was performed in order to analyze the effect of using a lagged weight windows approach on a problem consisting of optically thick materials, allowing for slow changes in the scalar flux. In this problem the material has an opacity of $\sigma = 300T^{-3}$ cm^{-1} with T in keV. The initial temperature is 1 eV and there is a boundary source at 1 keV on the left of the problem. This problem is optically thick everywhere

with any reasonable mesh.

Figure 3.1 shows the material temperature at $t = 10$ ns using different solution techniques. The number within the parenthesis seen in the legend represents the nominal number of particles simulated per time step of size $\Delta t = 0.01$ ns. The solution using 1 million particles per time step is the reference solution in the figure. From the plot it can be observed that the solution obtained using the lagged weight windows approach is at least as accurate as, if not more accurate than, the solution obtained without. The region behind the wavefront is much noisier in the no weight windows solution with 5×10^4 particles per step than in the weight windows solution with the same number of particles per step. Additionally, in the 5×10^4 particles per step simulation, the solution obtained without weight windows took 5203 seconds, while the weight windows solution only took 881 seconds, 1/6th the original runtime.

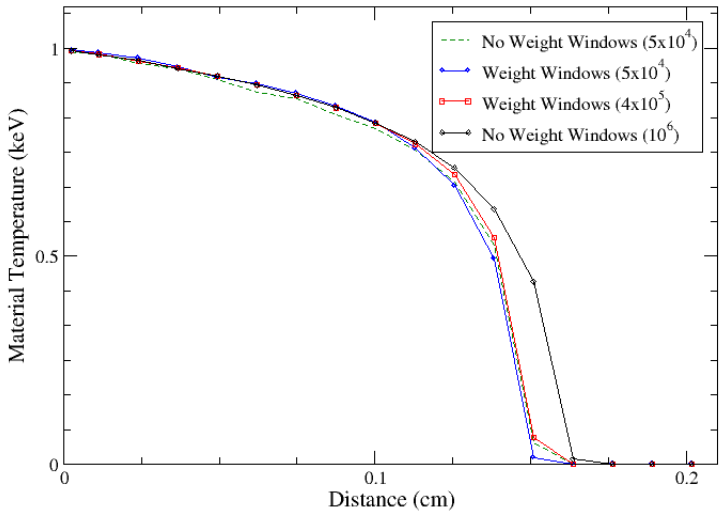

Figure 3.1: 1-D Marshak wave material temperatures at 10 ns. The numbers in parenthesis are the number of particles per time step.

Figure 3.2 depicts the number of particles entering each zone at t = 10 ns for the 5×10^4 particles per step simulations. The solution with weight windows shows a much more uniform distribution of particles than the solution without. Also, because the weight windows technique can terminate particles that have too small a weight, there are many fewer particle tracks in the weight windows solution. Given that in this Marshak wave problem the scalar flux is slowly evolving, the lagged weight windows technique successfully leads to a more uniform Monte Carlo particle flux, as predicted.

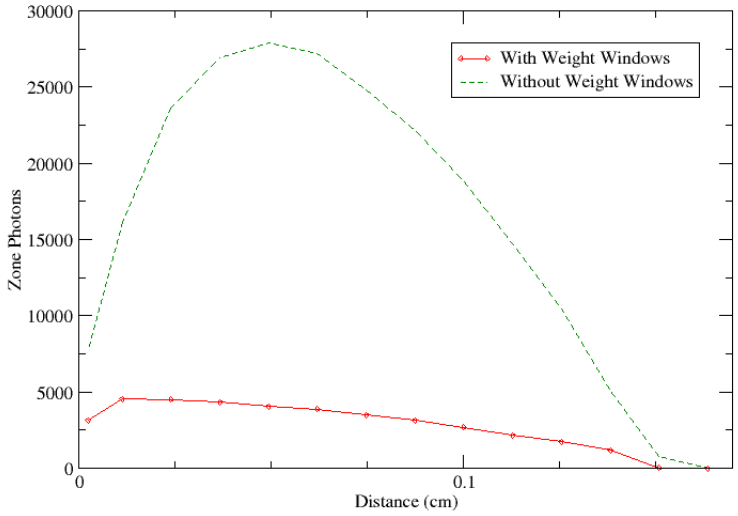

Figure 3.2: Number of particles entering each zone during the last step of the 5×10^4 particles per step simulations shown in Figure 3.1.

3.1.2 2-D Crooked Pipe Test Problem

A 2-D crooked pipe simulation was also performed to analyze the effects of the lagged weight windows technique. The schematic for the simulation is seen in Fig. 3.3. The

configuration is composed of two different types of materials, one which is optically thin, and one which is optically thick. There is a 1 keV blackbody source at the $x = 0$ plane. In the optically thin material, particles can stream through many spatial zones during a time step. This leads to a large change in the scalar flux at each time step near the wave front, and therefore the simulation is expected to experience spikes in the particle flux towards the particle wave front.

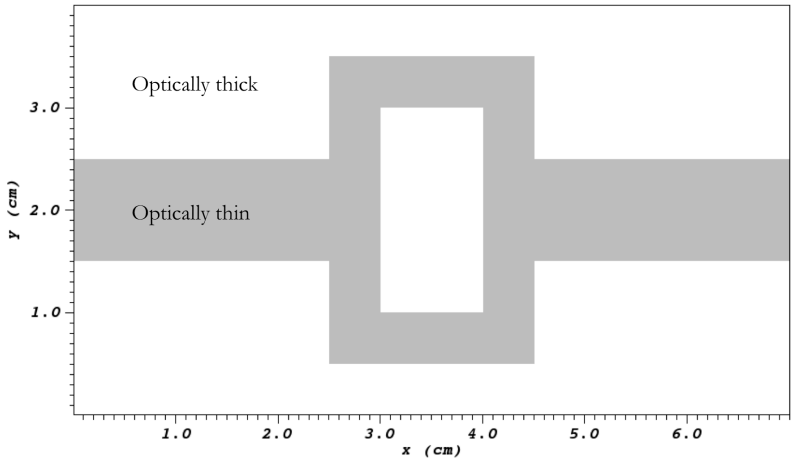

Figure 3.3: 2-D Cartesian crooked pipe schematic.

Figure 3.4 depicts a line-out at y = 2 of the number of particles entering each zone with and without the use of weight windows at two different times, 0.0114 ns and 0.0512 ns. For this problem the ratio of the splitting weight to the roulette weight is 5; that is particles with a weight greater than 2.5 times the window center are split and particles with a weight less than 1/2 the window center undergo Russian roulette [10, 11]. The solution obtained without weight windows for the two different time steps does not illustrate complete uniformity with the particle flux, but as expected, the particle flux is larger towards the left

plane of the simulation, where many particles are originating from the source. Compared to the material used during the Marshak Wave simulation, the opacity of the optically thin portion of the crooked pipe simulation is much smaller, and the solution obtained using the lagged weight windows technique exhibits spikes in the number of photons entering into each zone towards the wave front.

Figure 3.5 depicts a line-out at y = 2 of the particle flux obtained using a much larger split to roulette ratio (in effect this means there is much more splitting and less roulette). The plot depicts a much more significant spike in the number of photons entering into each zone. Though the total number of photons in the problem is smaller, a large fraction of the total photons are in the spike; this effect can be seen in Fig. 3.6 where the particle flux is scaled by the average particle flux. This is undesirable because in this problem one would expect to see a uniform particle flux if the proper weights were used. This is one example where using the lagged particle flux, despite its simplicity, is not as effective as other treatments that use an auxiliary calculation to estimate the scalar flux to be used for the weight windows.

3.1.3 Preventing Splitting in Optically Thin Materials

To address the spike in the particle flux magnitude exhibited in the crooked pipe test problem, we propose specifying a condition which would limit the amount of splitting in optically thin materials. This can be achieved by choosing to split a particle only if the width of the current cell (within the mesh) is greater than the mean free path of a particle. I.E. the following must be true in order for a particle to split:

$$dx > C\xi, \tag{3.4}$$

$$dy > C\xi, \tag{3.5}$$

$$dz > C\xi, \tag{3.6}$$

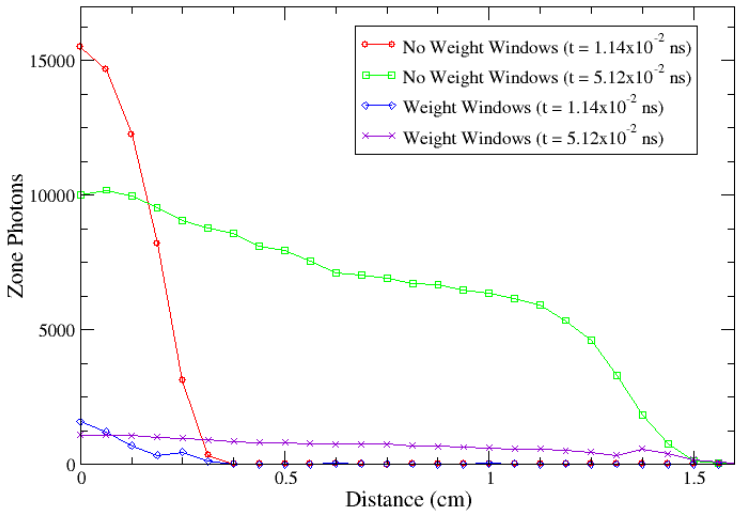

Figure 3.4: 2-D Crooked pipe particle flux using a split/roulette ratio of 5.

where dx, dy, and dz are the cell widths in the cartesian coordinate system, ξ is the average distance a particle travels before undergoing an interactions (also known as the mean free path), and C is a constant specified by the user. In optically thick materials, the cell width will almost certainly be greater than the mean free path of the particle (for reasonably sized meshes), thus this added condition will not affect the results previously seen for the 1-D Marshak Wave. On the other hand, this added condition should prevent the particle flux spikes in optically thin materials, as seen in Figs. 3.4 - 3.6, which emanated from the rapid change in the radiation intensity.

Figure 3.7 displays a line-out at y = 2 of the number of particles entering each zone with and without the use of weight windows at two different times, 0.0114 ns and 0.0512 ns, with the added condition. The image shows that the new condition successfully prevents the occurrence of spikes in the particle flux and resulted in a more uniform distribution of particles.

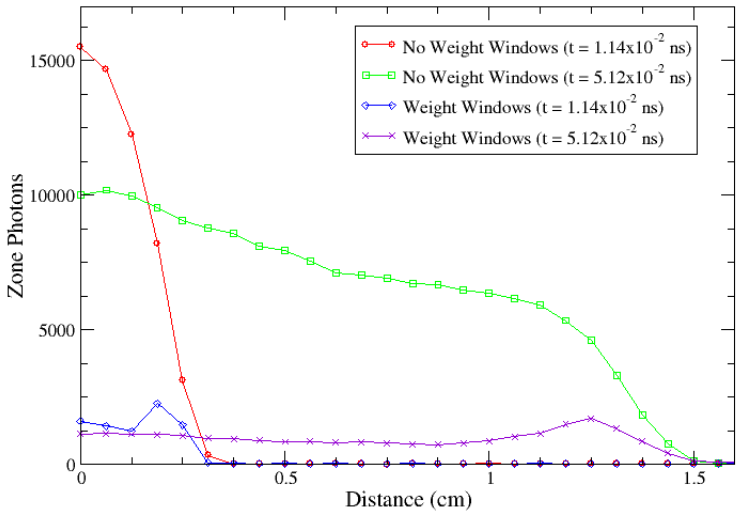

Figure 3.5: 2-D Crooked pipe particle flux using a split/roulette ratio of 5000.

3.2 Deciding What to Do with the Russian Roulette Energy

Upon fixing the spike in the particle flux for optically thin materials, it was discovered that an issue was causing an unphysical increase of the material temperature within the crooked pipe problem. Previously, when a particle was terminated due to Russian Roulette, its energy-weight would be temporarily stored within a "bank" unique to each zone. When a particle survives Russian Roulette, energy is drawn from the bank and given to the particle. If energy remains in the bank at the end of the time step, that energy is distributed between all census particles in the zone, however, if there are no particles, then the energy is deposited into the material, causing an increase in material temperature. We presume that unphysical heating may be occurring from having an excessive amount of bank energy at the end of a time step, with no census particles to distribute it to. We believe this results in deposition of all the energy into the material, leading to unnatural

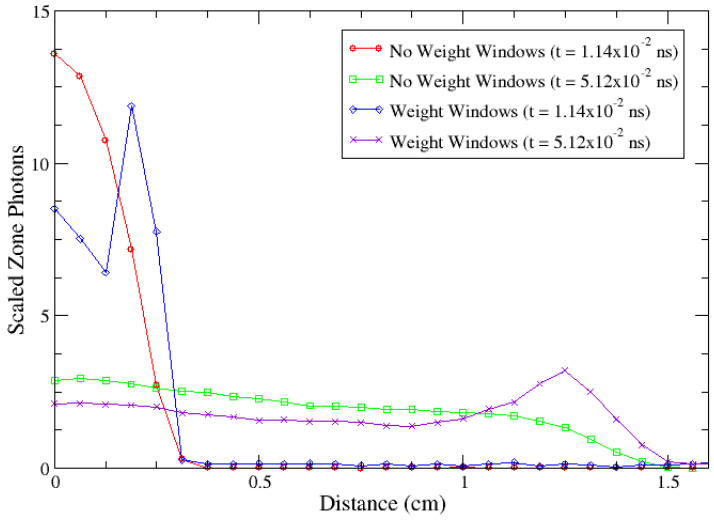

Figure 3.6: The 2-D Crooked pipe particle flux from Fig. 3.5 normalized by the average particle flux. A value of one means a zone has the average number of photons entering.

heating. This challenged us to develop an alternative method for deciding what to do with the energy residing in the bank. We thought of four:

Method 1 - Bank energy is distributed between all census particles in the current zone. If there are no particles then the energy is deposited directly into the material. This is the original method.

Method 2 - Bank energy is distributed globally to all the census particles depending on the ratio between a particle's current energy and the total census energy.

Method 3 - Bank energy is distributed between all census particles in the current zone. If there are no particles then the energy is distributed globally to all the census particles.

Method 4 - Bank energy is distributed between all census particles in the current

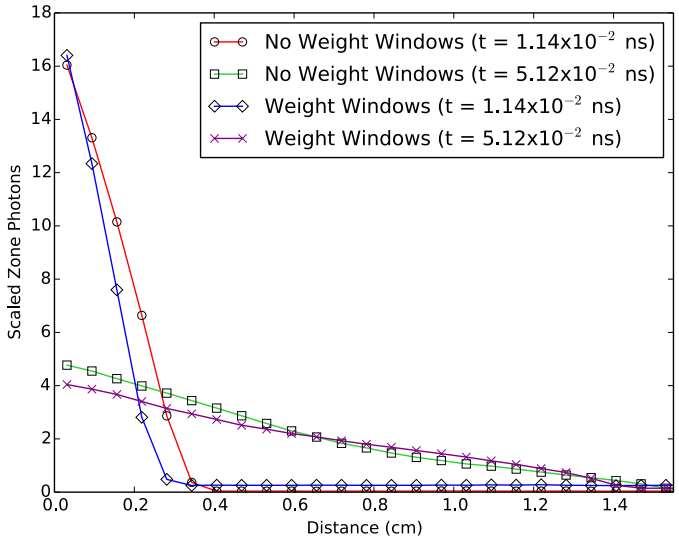

Figure 3.7: 2-D Crooked pipe particle flux using a split/roulette ratio of 5, normalized by the average particle flux. These plots were obtained with the added condition, which prevents splitting in thin materials.

zone. If there are no particles, then additional particles are created and the bank energy is distributed equally.

The four methods were tested on the 1-D Marshak wave problem. Figure 3.8 displays the material temperature obtained using the various methods with 5×10^4 particles per time step. In addition, a solution without variance reduction and a "converged" solution using 3×10^6 particles per time step are displayed. The image clearly shows that method 2 greatly underestimates the location of the wavefront. As a further comparison, a figure of merit was calculated, which is defined as:

$$\text{FOM} = \frac{1}{\epsilon^2 \bar{t}}, \tag{3.7}$$

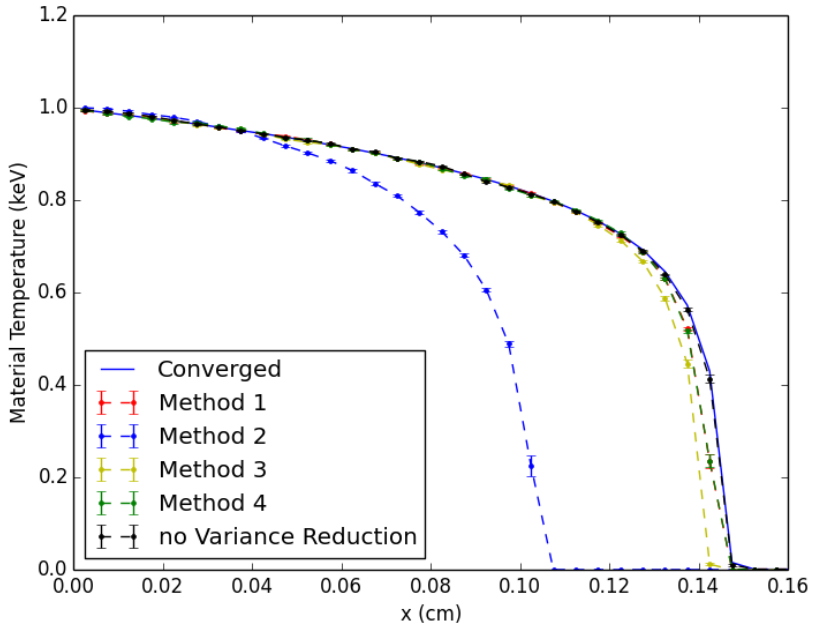

Figure 3.8: Comparison of the material temperature obtained using the various methods for handling the roulette bank energy.

where $\bar{t}$ is the average runtime of 20 independently seeded calculations. ϵ is the average absolute error in the material temperature for 20 independently seeded simulations i.e.

$$\epsilon = \frac{\sum_{i=1}^{20} |T_i - T_{\text{converged}}|}{20}, \tag{3.8}$$

where T is the material temperature. The FOM is displayed in Fig. 3.9. It is clear that methods 1, 3 and 4 outperform IMC without variance reduction, however we feel that method 4 is the most consistent, especially considering the heating issue when using method 1 on the crooked pipe problem. Additional testing on the crooked pipe problem using method 4 resulted in no instances of unphysical material temperatures.

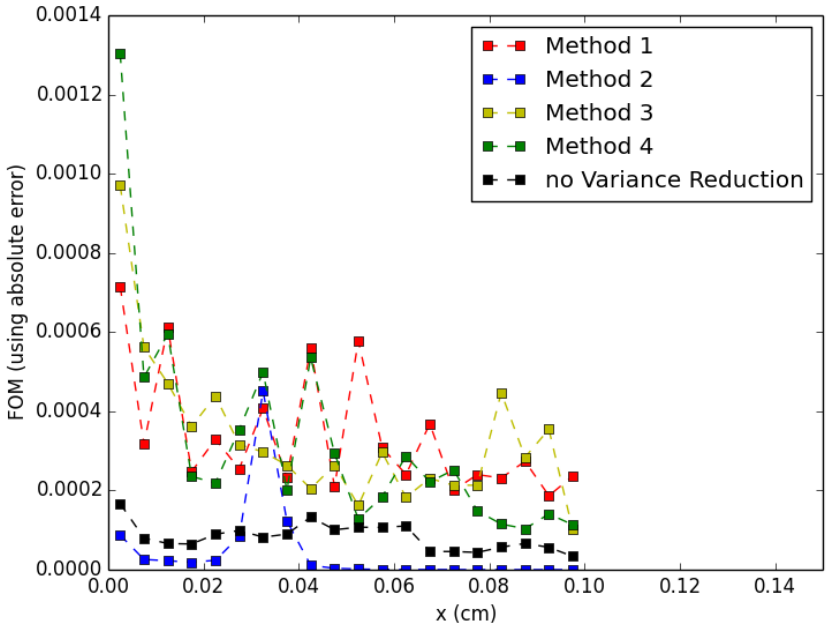

Figure 3.9: Figure of merit comparing the IMC efficiency using the various methods for handling the roulette bank energy.

3.3 Additional Considerations for Multi-Region Problems

Additional complications have been discovered at the interface between thick and thin materials. At these interfaces, an abnormal amount of heating occurs, resulting in conflicting numerical solutions. This problem was first discovered in the 2-D crooked pipe results. Line-outs of the material temperature and the zone photons were obtained for various simulations at the time, $t \approx 0.5$ sh at $y \approx 1.0$ cm. The material temperature line-outs are displayed in Fig. 3.10. Figure 3.10 shows that the solutions obtained with weight windows are hotter than those obtained without, which is concerning. It is our belief that distributing the bank energy to census photons may allow for unphysical heating due to thermal energy traveling too far. We have not accounted for how far a photon has travelled in time (relative to the beginning of the time step) before it underwent Russian Roulette.

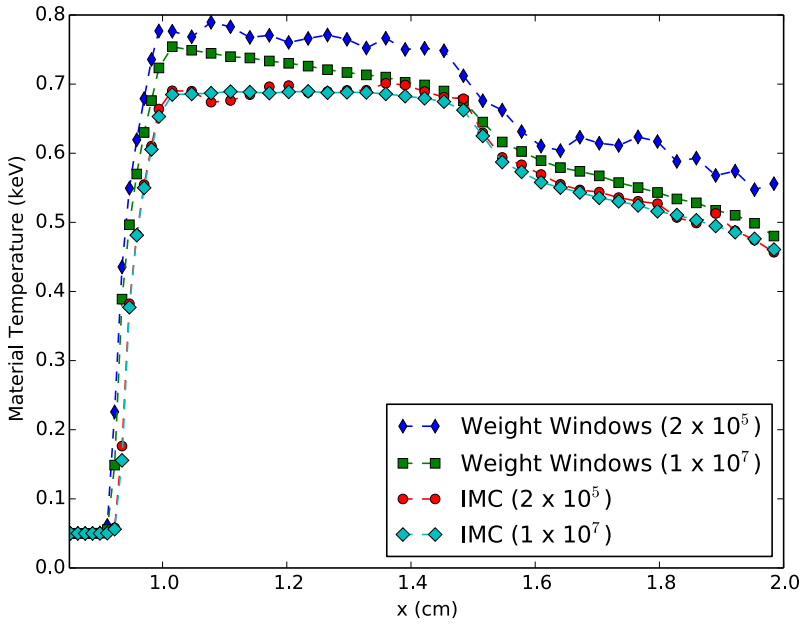

Figure 3.10: Line-out at $y \approx 1.0$ cm of the material temperature at $t \approx 0.5$ sh for the crooked pipe problem. The number in parenthesis is the number of particles emitted per time step.

4. SUMMARY AND CONCLUSIONS

To conclude, two methods were developed, which aimed to improve thermal radiative transfer Monte Carlo simulations. One method involved adding a volumetric dependence to the IMC "Fleck" factor, which increased the amount of photon re-emission in zones that were volumetrically small compared to the zone that a particle was emitted in. This method intended to eradicate the presence of anomalous heating, which can occur when using too few of particles in meshes that have very large changes in zone volumes (e.g. RZ meshes as shown in chapter 2). The method did successfully remove the abnormal heating at the r = 0 axis, where the zone volumes are minuscule compared to where the majority of particles are born, however, the loss in accuracy (due to changing the actual physics of the problem) was too large to bear. Thus, an additional condition was introduced, negating the use of a volume-dependent Fleck factor when there is enough particle contributions within a given zone. This addition leads to numerically accurate solutions as the number of particle histories approaches infinity, however we discovered that the loss in accuracy due to the added volume dependence remained larger than the expected statistical noise obtained without using this method. We believe that imposing a reduction limit to the Fleck factor may improve this methods effectiveness, however this has not yet been studied.

The second method utilized a common variance reduction method known as weight windows. Weight windows is widely used in the Monte Carlo community, however the procedure for obtaining an optimal weight window center remains open for debate. Our scheme used the radiation intensity from the previous time step for the center of the weight window, dubbing it a "lagged" weight window center. As shown in chapter 3, this simple approach worked very well for problems containing optically thick materials, where the radiation intensity changes very little between reasonably sized time steps. However, for

problems that contained optically thin materials, spikes in the photon count would occur at the wave front where the radiation intensity is changing rapidly. This is an undesirable side-effect considering that a uniform particle flux is typically desired when seeking global accuracy. Thus, a condition was added, which successfully allows particle splitting in only thick regions.

Additionally, abnormal heating was discovered in a 2D test problem, which was presumed to be due to the procedure for dealing with the "bank" energy accumulated from Russian Roulette. Thus, we analyzed four distinct approaches for adding the bank energy into the problem. From our study, we concluded that the most logical approach was to distribute the bank energy associated with each zone to the census particles of said zone, and if no particles reached census, then additional census particles would be created. This approach successfully removed the anomalous heating and paved the way for the possible increases in computational efficiency in multi-region problems, containing both optically thick and thin materials. However, we recently discovered that distributing the bank energy to census particles can cause a bias, which allows thermal energy to travel too far.

REFERENCES

[1] N. Metropolis, "The beginning of the Monte Carlo method," *Los Alamos Science*, vol. 15, no. 584, pp. 125–130, 1987.

[2] J. A. Fleck, Jr. and J. D. Cummings, "An implicit Monte Carlo scheme for calculating time and frequency dependent nonlinear radiation transport," *J. Comput. Phys.*, vol. 8, pp. 313–342, 1971.

[3] A. B. Wollaber, "Four decades of implicit Monte Carlo," *Journal of Computational and Theoretical Transport*, vol. 45, no. 1-2, pp. 1–70, 2016.

[4] A. Wollaber, *Advanced Monte Carlo Methods for Thermal Radiation Transport*. PhD thesis, University of Michigan, University of Michigan, Apr. 2008.

[5] R. E. Caflisch, "Monte Carlo and quasi-Monte Carlo methods," *Acta numerica*, vol. 7, pp. 1–49, 1998.

[6] T. E. Booth and J. S. Hendricks, "Importance estimation in forward Monte Carlo calculations," *Nuclear Technology/Fusion*, vol. 5, pp. 90–100, January 1984.

[7] M. A. Cooper, *An automated variance reduction method for global Monte Carlo neutral particle transport problems*. PhD thesis, Univ. of Michigan, 1999.

[8] T. Becker and E. Larsen, "The application of weight windows to "global" Monte Carlo problems," in *Proceedings of the 2009 International Conference on Advances in Mathematics, Computational Methods, and Reactor Physics, Saratoga Springs, New York*, pp. 3–7, 2009.

[9] C. J. Solomon, A. Sood, T. E. Booth, and J. K. Shultis, "A priori deterministic computational-cost optimization of weight-dependent variance-reduction parameters for Monte Carlo neutral-particle transport," *Nucl. Sci. Eng.*, vol. 176, pp. 1–36, 2014.

[10] F. B. Brown, "Fundamentals of Monte Carlo particle transport," Tech. Rep. LA-UR-05-4963, Los Alamos National Laboratory, 2005.

[11] M. Cimino (dir.), *The Deer Hunter*. Universal Pictures, 1978.

[12] J. T. Landman and R. G. McClarren, "A Volume-Dependent Fleck Factor for Added Robustness in Implicit Monte Carlo Calculations," *M&C*, April 2015.

[13] J. T. Landman, R. G. McClarren, J. Madsen, and A. Long, "Analysis of Lagged Weight Windows for Implicit Monte Carlo Variance Reduction," *ANS Winter Meeting*, 2014.

[14] R. G. McClarren, T. M. Evans, R. B. Lowrie, and J. D. Densmore, "Semi-implicit time integration for P_N thermal radiative transfer," *J. Comput. Phys.*, vol. 227, no. 16, pp. 7561–7586, 2008.

[15] F. Graziani and J. LeBlanc, "The crooked pipe test problem," tech. rep., UCRL-MI-143393, 2000.